



Polymer Composite @ Nano TiO₂/LiBF₄ as an Electrospun Fiber Nano Composite Electrolyte: Preparation, Characterization and Electrical Properties

Emad M. Masoud¹ · Amir I. Abdelsamea² · Mona N. Elsabagh² · Sarah L. Abdelaziz² · Abdallah M. Abbas²

Received: 12 February 2023 / Accepted: 17 March 2023 / Published online: 12 April 2023

© The Author(s), under exclusive licence to Springer Science+Business Media, LLC, part of Springer Nature 2023

Abstract

As a new trial of overcoming constraints regarding degradation stability, amorphous structure nature, high potential of breakdown and band offsets process ability and reproducibility of polymer composite electrolytes used in energy storage systems such as lithium ion batteries was here reported. In presence of three different polymers, PMMA, PVDF-co-HFP and PEO, with a respectively molar ratio of 1:1:0.5, electrospun fibers nano composites electrolytes containing different concentrations of nano TiO₂ filler and lithium tetrafluoro borate salt were successfully synthesized using electrospinning technique. All results of structure characterization confirmed that the sample containing 12 wt.% nano TiO₂ filler (NPEC4) has the optimized structure for the electrical properties performance. This sample exhibited low crystallinity, high thermal stability, suitable pore diameter and fiber diameter of its electrospun. The same sample showed high ionic conductivity ($\sigma_{AC} = 1.08 \times 10^{-3} \Omega^{-1} \text{ cm}^{-1}$) at room temperature. Electrical properties of this sample, in addition to a comparison with previous studied similar electrolyte systems, exhibited the ability of this electrospun fiber nano composite electrolyte to be used as a promised solid electrolyte for lithium-ion batteries application. All results were collected and discussed.

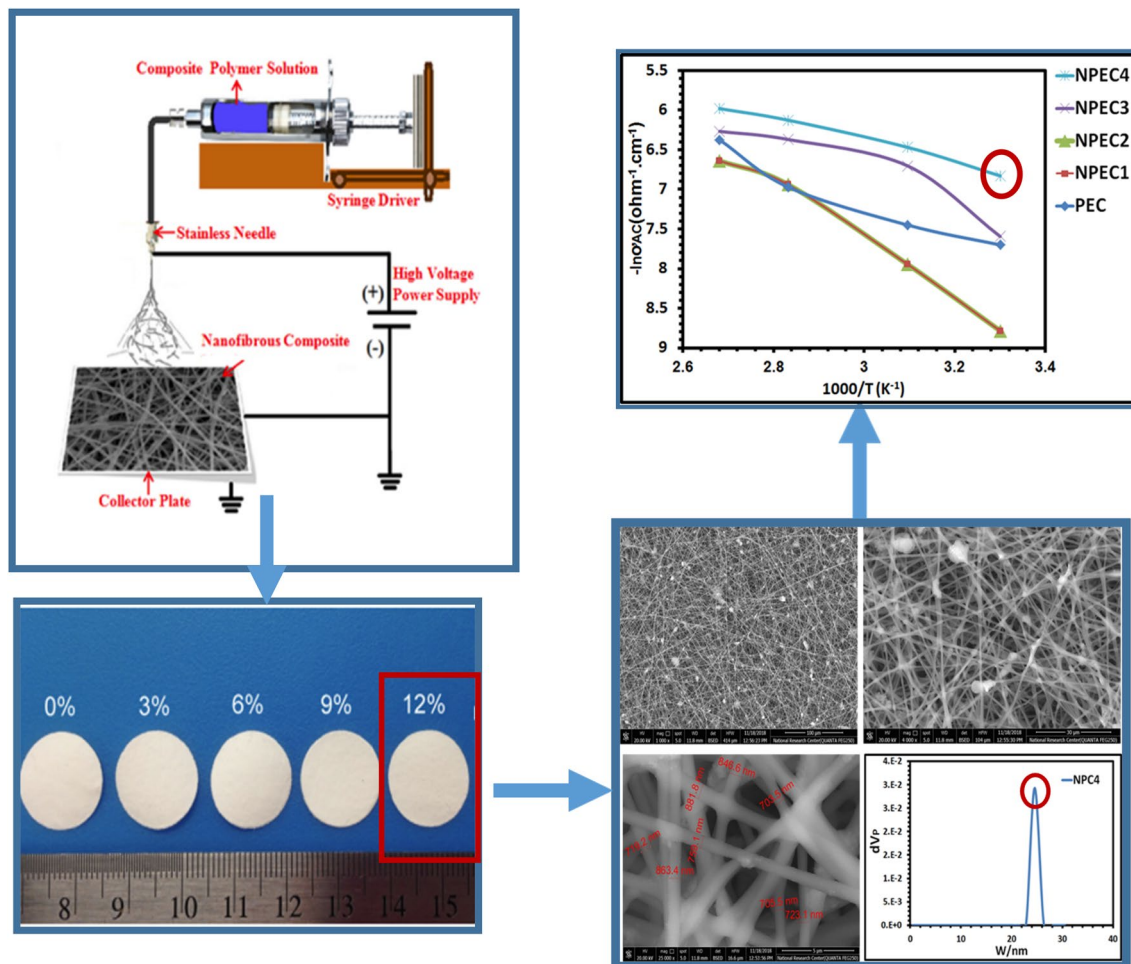
✉ Emad M. Masoud
emad.youssef@iu.edu.sa

¹ Department of Chemistry, Faculty of Science, Islamic University of Madinah, 42351 Madinah, Saudi Arabia

² Department of Chemistry, Faculty of Science, Benha University, Benha 13518, Egypt

Graphical Abstract

One electrospun nano fiber composite containing 12 wt.% nano TiO₂ filler exhibited structural promised properties supporting the electrical properties performance.



Keywords Electrospun fiber · Electrical properties · Polymer nano composite electrolyte · Porosity · Lithium ion batteries

1 Introduction

Both of environmental pollution and global warming have stimulated extensive explorations of renewable clean energy (solar, wind, and hydrogen energies et al.) However, the discontinuous nature of renewable energies requires efficient energy storage units to supply continuous and stable energy, including batteries, fuel cells, and supercapacitors. Many scientific trials using different energy units [1–12] were performed to overcome that nature. Lithium-ion batteries have received considerable attention as the most popular energy storage system for a wide variety of portable electronic devices including laptops, digital cameras, and cell phones with the worldwide market valued at ten billion dollars. They are also one of the most promising candidates

as the large-scale power source for electric vehicles and emerging smart grids because they have several important advantages including high energy density, no memory effect, long cycle life, and low self-discharging [4, 13, 14]. New battery components need development to achieve good performance Li-ion batteries with low cost and high safety [15, 16]. Many polymeric materials as solid polymer electrolyte were used for lithium ion batteries application. As examples: poly(propylene oxide) (PPO) [17, 18], Polymethylmethacrylate (PMMA) [19], poly(ethylene oxide) (PEO) [20] and their various copolymers [21], polyphosphazene (MEEP) [22], polyketones [23], polyethyleneglycol [24], polyurethane and polyether blends [25], polyvinylidene fluoride (PVdF) and their different copolymers with hexafluoropropylene (HFP) or trifluoroethylene (TrFE) [26]; many

different polymer nano composites were also used [27]. Till now, different constraints relating to degradation stability, amorphous structure nature, high potential of breakdown and band offsets process ability and reproducibility still needed to be solved [28]. Many trials were performed to overcome the above mentioned constraints; by using pure or mixed types of polymer (blending of two polymers) to form matrixes which can exhibit good structure for oxidation–reduction processes of lithium ion batteries application. The main problem of this target is how to mix polymers (blending) in a definite type and molar ratio concentration, which can deliver suitable textural structure, including high amorphicity and a good thermal stability. Some polymers, as following, were used pure as polymer electrolytes and exhibited some advantages, beside some of disadvantages. PMMA is one of the most important polymeric materials that has different energy applications, such as electrolytes for Li-ion batteries. Different methodologies were used to adjust the different properties of PMMA electrolytes. The best results were achieved using ionogel composite containing poly (methyl methacrylate) (PMMA) in presence of various types of organic salts [29–32]. Also, one of the most important polymeric materials is Poly (vinylidene fluoride-co-hexafluoro propylene) (PVdF-co-HFP) [33–35]. Although polymer electrolytes of PVdF-co-HFP achieved good thermal stability at different temperatures, they showed only ionic conductivity at high temperature with flexible nature, and as a result poor thermal stability. Polyethylene oxide (PEO) is also one of the good polymeric material for electrolyte membranes because it has high electrochemical stability and also exhibits good compatibility in presence of various lithium salts [36–38]. At the same time, ionic conductivity value of the PEO-electrolyte is insufficient for application because its chains have high crystallinity value. According to literature, Different fillers such as TiO_2 , SiO_2 , Al_2O_3 , ZnO , etc., were used to enhance both of the conductivity value and electrochemical stability behavior of polymer electrolytes [39–41]. These fillers can reduce the ion paring due to the presence of Lewis acid surface groups and as a result increasing the conductivity value. Additionally, these fillers can also achieve interphase stabilization and decrease the resistance value with electrodes [42–44]. In this paper, as a new methodology, polymer nano composite electrolyte containing three different polymers; PMMA, PVdF-co-HFP and PEO at the same time will be prepared in a definite molar ratio as a trial to overcome the last above observed constraints of these polymers when used as pure ones. The aim of this blending is to decrease the crystallinity percent, especially for PVdF-co-HFP and PEO polymers and also to enhance matrix thermal stability, which will make the composite having good electrochemical stability value as reported in previous studies [19]. The problem of mixing three different polymers to form suitable matrix for the charge motion is

how to determine the molar ratio composition that can keep finally the good physical properties of polymers composite, such as its mechanical property. Additionally, nano TiO_2 will be added in different concentrations to help in enhancing the textural structure (especially for matrix amorphicity, thermal stability and new pathways of charger migration) through well interactions with polymers matrix. Moreover, the methodology of pores creation, which can induce more favorable conduction pathways for the charge carriers, will also be performed to prepare electrospun fiber of these polymers matrix using electrospinning technique.

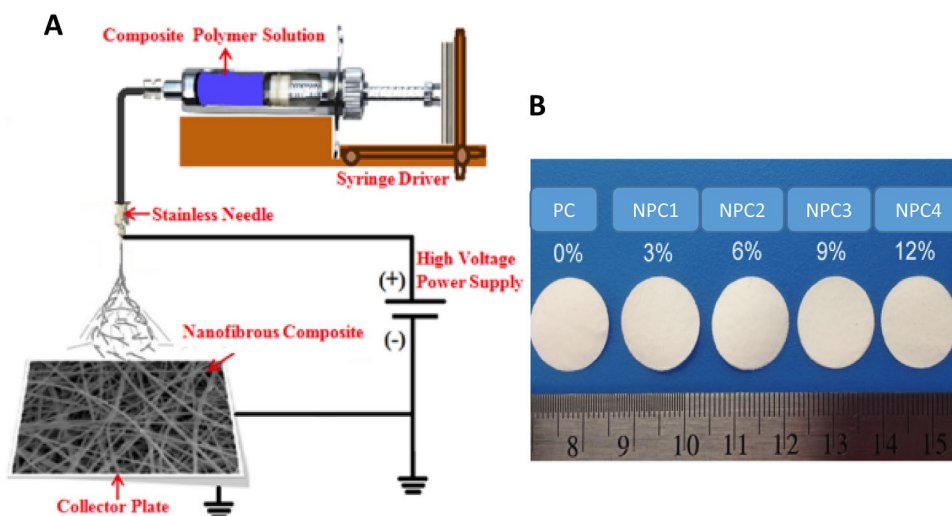
2 Experimental

Materials: PMMA (Polymethylmethacrylate, M.wt = 350,000, Sigma-Aldrich, 99.99%), PVdF-co-HFP (polyvinylidene fluoride-co-hexafluoro propylene M.wt = 300,000, Sigma-Aldrich, 99.99%), PEO (polyethylene oxide, M.wt = 600,000, Sigma-Aldrich, 99.99%), TiO_2 (Titanium dioxide, Aerosil PF2, particle size = 20 nm, Sigma-Aldrich, 99.99%), LTFB (Lithium tetrafluoro borate, Sigma-Aldrich, 99.99%) and DMF (N, N Di-methyl formamide, Sigma-Aldrich, 99.99%).

2.1 Electrospun Fiber Synthesis of Pure Polymer Composite, Polymer Nano Composites and Polymer Nano Composites Electrolytes

To obtain electrospun fiber of pure polymer composite, after many trials of optimization for the polymers molar ratio, three different polymers of PMMA, PVdF-co-HFP and PEO in a respectively molar ratio of 1:1:0.5 were dissolved in 23 ml DMF at 40 °C. The viscous solution was stirred overnight before electrospinning process. As shown in Fig. 1A, a high voltage of 20 kV is applied using a power supply (Gamma) between the electrospinning solution contained in the syringe and the grounded collector plate. When the voltage reached a critical value, the electrostatic force overcomes the surface tension of the pendant drop of the polymer solution at the tip of the stainless needle and a liquid jet is ejected. Fibers deposit on the grounded collector plate and form a non-woven structure. Electrospun fiber of pure polymer composite was collected as a free-standing membrane (Fig. 1B). The feeding rate value was 1 ml/h and the distance between tip and collector was 12 cm. To get rid of solvent, drying of fiber membrane was performed at 60 °C for 24 h. Following, different concentrations (3, 6, 9, 12 wt.%) of nano TiO_2 was added using the same above method to obtain polymer nano composites electrospun fibers. The addition of more than 12 wt.% of nano TiO_2 made the electrospun fibers having not stable mechanical property. The thickness of all membranes were measured using a micrometer screw gauge

Fig. 1 Schematic diagram for **A** preparation method of electrospun fibers and **B** their photographs



and found around 60 μm . Also, polymer nano composite electrolytes electrospun fibers were prepared by polymer nano composites fibers soaking process in a liquid electrolyte containing Lithium tetrafluoro borate (LTFB) salt (1 M lithium tetrafluoroborate (LTFB) in ethylene carbonate and diethyl carbonate (EC + DEC, 1:1 by volume).

All prepared fibers were denoted as following: PC, NPC1, NPC2, NPC3, NPC4, PEC, NPEC1, NPEC2, NPCE3, NPEC4 for pure polymer composite, polymer composite containing 3 wt.% nano TiO_2 , polymer composite containing 6 wt.% nano TiO_2 , polymer composite containing 9 wt.% nano TiO_2 , polymer composite containing 12 wt.% nano TiO_2 , polymer electrolyte composite, polymer electrolyte composite containing 3 wt.% nano TiO_2 , polymer electrolyte composite containing 6 wt.% nano TiO_2 , polymer electrolyte composite containing 9 wt.% nano TiO_2 and polymer electrolyte composite containing 12 wt.% nano TiO_2 , respectively.

2.2 Characterization of Samples

On a Diano (Cu-filtered $\text{CuK}\alpha$ radiation ($\lambda = 1.5418 \text{ \AA}$)) energized at 45 kV, and 10 mA, X-ray diffraction analysis was done. The samples were characterized in a range from $2\theta = 10$ to 70° , at room temperature. The Fourier transform infra-red spectra were measured in a range between 400 and 4000 cm^{-1} by a Bruker—FT-IR. In air atmosphere and a temperature range of 303–873 K, thermal gravimetric (TG) and differential scanning calorimetry (DSC) analyses were performed. The heating rate was $10^\circ\text{C}/\text{min}$. using Shimadzu DSC-60H. JOEL scanning electron microscopy (JSM-35CF) was used to investigate the composites nature. To investigate the composites porosity, Brunauer–Emmett–Teller (BET) nitrogen adsorption–desorption isotherm was performed with a Micrometrics (ASAP2020) apparatus. Using a programmable automatic LCR bridge (Model RM 6306 Phillips

Bridge), electrical properties were also studied in a temperature range from 303 to 373 K and a frequency one from 100 Hz to 1 MHz.

3 Results and Discussion

Figure 2 displayed X-ray diffraction patterns of A1: PVdF-co-HFP; A2: PEO and PMMA and B: PC, TiO_2 , NPC1, NPC2, NPC3 and NPC4. Figure 2A1, A2 showed the semi-crystalline structure of both PVdF-co-HFP (Peaks in a range of $2\theta = 10$ –25 degree) and PEO (Peaks in a range of $2\theta = 25$ –35 degree), and the amorphous nature of PMMA. Figure 2 B showed absence of all crystalline peaks of the two polymers (PVdF-co-HFP and PEO) in the PC sample. This can be attributed to the good interactions of each. Moreover, the figure also showed the addition effect of different nano TiO_2 filler concentrations on the PC sample containing the three mixed polymers. The addition of nano TiO_2 filler showed crystalline peaks, which corresponding to the crystalline phase of TiO_2 , in all NPC samples. The NPC4 sample showed the lowest intensity of these peaks which also due to the good interactions of nano filler (12 wt.%) with the PC matrix. This interaction process can be represented as in Fig. 3.

Figure 4 showed FT-IR patterns of A: PVDF-co-HFP, PEO and PMMA; B: PC and C: TiO_2 , NPC1, NPC2, NPC3 and NPC4. The A and B patterns showed a shift of the main band of each polymer in the PC sample, confirming the good interactions between the three polymers as shown above from X-ray analysis. The wave number value assignment of each polymer main band, in addition to its corresponding shift one in PC sample were investigated, Table 1. In contrast, the C patterns also showed a shift of TiO_2 main band in NPC samples, confirming the good interactions between the nano filler and the polymers matrix as also confirmed in

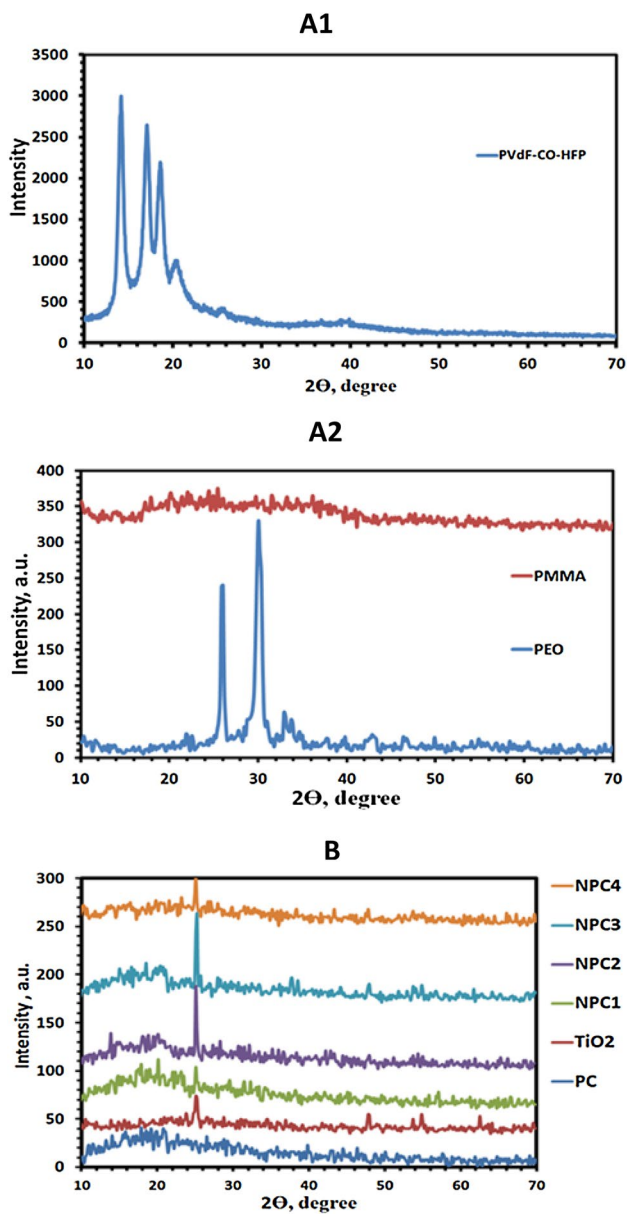


Fig. 2 X-ray diffraction patterns of **A1** PVDF-co-HFP; **A2** PEO and PMMA and **B** PC, TiO₂, NPC1, NPC2, NPC3 and NPC4

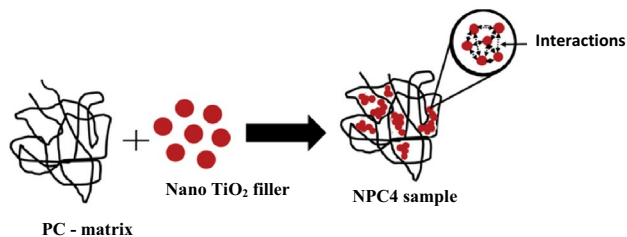


Fig. 3 Schematic diagram illustrating the nano filler interactions with the three mixed polymers matrix

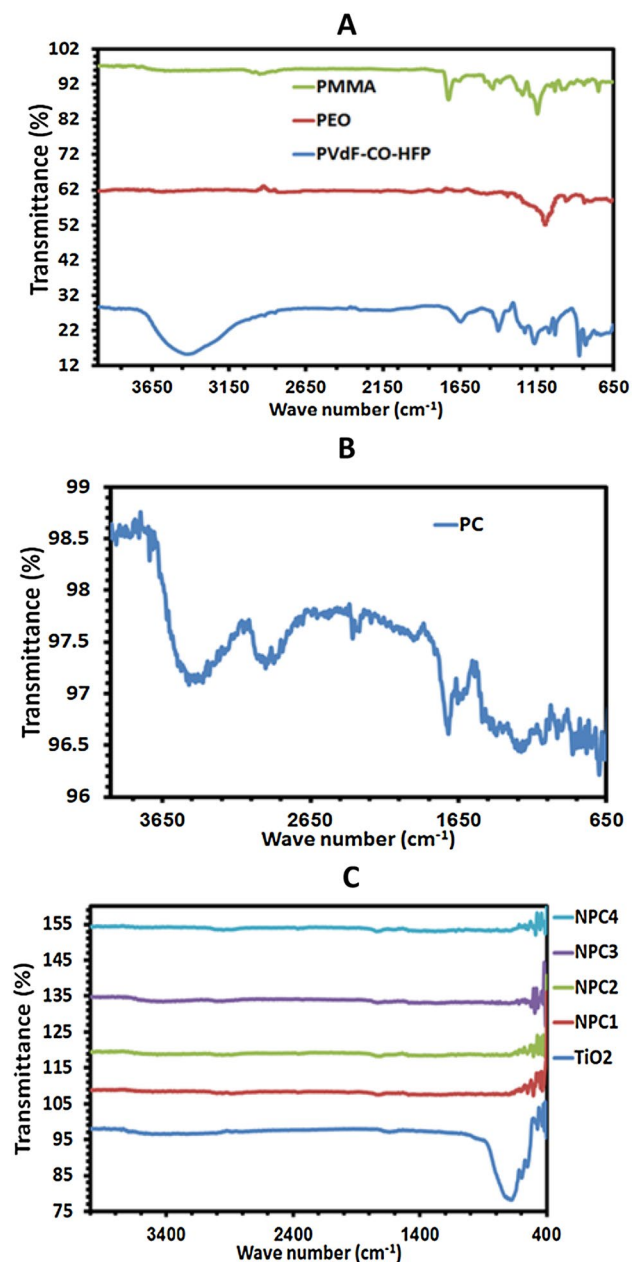


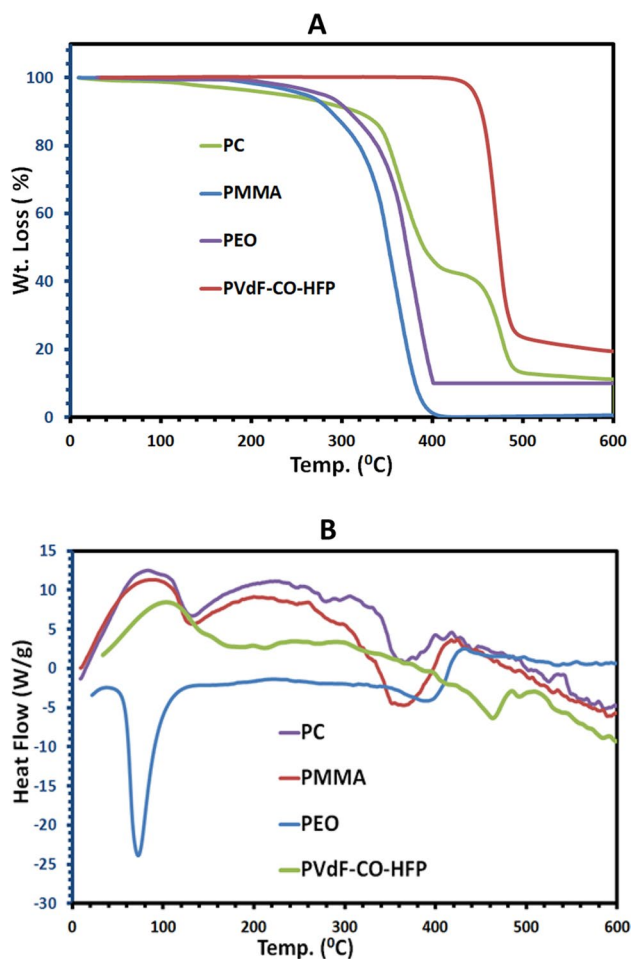
Fig. 4 FT-IR patterns of **A** PVDF-co-HFP, PEO and PMMA; **B** PC and **C** TiO₂, NPC1, NPC2, NPC3 and NPC4

X-ray analysis part. The wave number value assignment of the nano filler main band, in addition to its corresponding shift one in NPC samples were investigated, Table 1.

Figure 5A, B represents the thermal properties (TGA and DSC) of PVDF-co-HFP, PEO, PMMA and PC. Thermal stability investigation shows the using ability of membrane for lithium ion batteries application as a solid electrolyte. As shown in TGA curves, all samples represented weight loss in two regions. For the first region (from room temperature till 300 °C), all samples exhibited low weight loss, which can be attributed to the dehydration process and melting behavior.

Table 1 FT-IR spectral main band value assignment of PMMA, PEO, PVDF-co-HFP, TiO₂ and its corresponding shift one in PC and NPC samples

Sample	PMMA	PEO	PVDF-co-HFP	PC		
Wave number of a main characteristic band (cm ⁻¹)	1150–1250 (C–O–C stretching vibration)	1050–1160 (C–O–C vibration modes)	1200 (-CF ₂ group of PVdF-CO-HFP)	1162–1255, 1090–1193, 1226 for PMMA, PEO and PVdF-co-HFP, respectively		
Sample		TiO ₂	NPC1	NPC2	NPC3	NPC4
Wave number of a main characteristic band (cm ⁻¹)		690 (Ti–O stretching band)	551	542	543	539

**Fig. 5** A TGA and B DSC patterns of PVDF-co-HFP, PEO, PMMA and PC

For the second region (from 300 °C till around 400 °C for PMMA and PEO, and from 300 till 500 °C for PVdF-co-HFP and PC), all samples exhibited high weight loss due to the decomposition of polymeric matrix. Moreover, the four samples showed different thermal stability behavior against decomposition process. The PVdF-co-HFP sample showed high thermal stability behavior compared to the others with the following order: [PC > PEO > PMMA]. This shows that

Table 2 Values of melting temperature (T_m) and decomposition temperature (T_d) of PVDF-co-HFP, PEO, PMMA, PC, NPC1, NPC2, NPC3 and NPC4

T_d , °C	T_m , °C	Sample
464	272	PVDF-co-HFP
394	273	PEO
363	282	PMMA
413	279	PC
402	315	NPC1
394	314	NPC2
403	308	NPC3
411	319	NPC4

PC sample containing the three different polymers show very good thermal stability compared to pure PEO and PMMA. This also represents that the interactions between the three polymers, which was confirmed before from X-ray and FT-IR analyses have a good effect on the polymeric matrix structure in presence of this polymers molar ratio, which can support one of our main targets that can induce enhanced electrospun fiber for lithium ion batteries application as solid electrolyte. Additionally, DSC curves were also studied to confirm the suggested interpretation of weight loss processes of the four samples. The curves showed three main endothermic peaks at different temperatures for all samples. The first two ones were observed at the same region of TGA weight loss curves (from room till 300 °C), which can confirm the suggested presence of dehydration and melting processes of the samples. In contrast, the second one was also observed at the same region of TGA weight loss curves (from 300 till 500 °C). This also confirm the decomposition process of the polymers. Both of melting and decomposition temperatures values of all samples were exactly calculated and tabulated, Table 2. To also investigate the thermal stability behavior of PC sample with nano TiO₂ filler (NPC samples), TGA and DSC curves were also studied, Fig. 6A, B. The TGA curves showed regions of weight loss similar to what discussed before for PC sample. Addition of nano TiO₂ filler decreased the decomposition range of PC sample (Fig. 5A) from 350–500 °C to 350–420 °C, exhibiting that nano filler interactions with polymeric matrix can induce more amorphous structure as confirmed from X-ray analysis. Moreover,

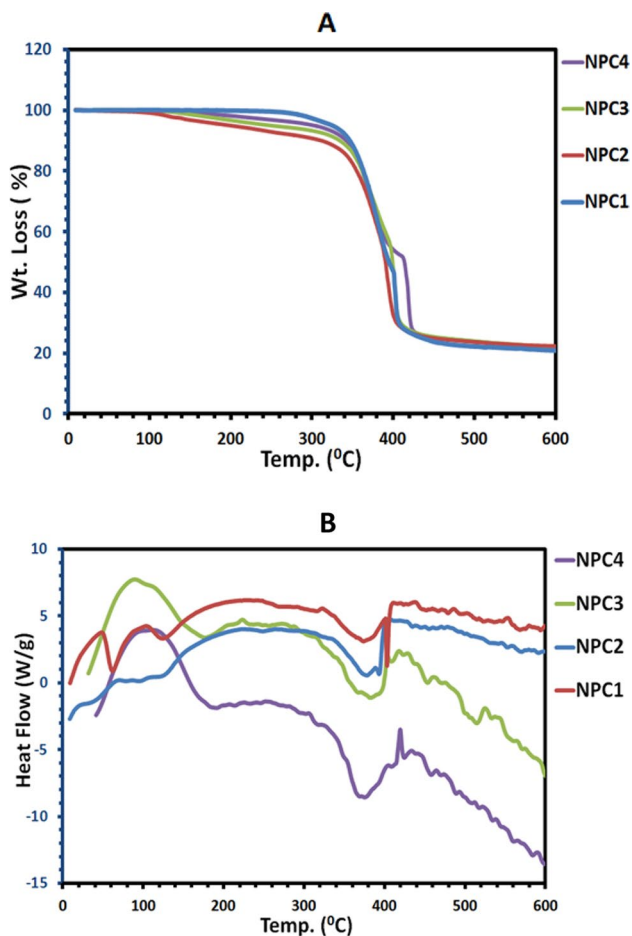


Fig. 6 **A** TGA and **B** DSC patterns of NPC1, NPC2, NPC3 and NPC4

the different concentrations of nano TiO₂ filler (NPC samples) showed small difference of thermal stability behavior. The NPC4 exhibited the end of high weight loss region at 420 °C compared to 400 °C for the others, which makes it having the highest thermal stability one. The DSC curves (Fig. 6B) showed endothermic peaks of chemical changes (dehydration, melting and decomposition) similar to what discussed before for PC sample. Also, all values of melting (T_m) and decomposition (T_d) temperatures for all NPC samples were exactly calculated, Table 2. The NPC4 sample exhibited the highest value of both melting and decomposition temperatures ($T_m = 319$ °C, $T_d = 411$ °C) compared to the others. Here, it is important to mention that NPC4 sample also exhibited the lowest crystalline nature compared to the others (X-ray analysis). This shows that this sample has an optimized structure for the electrical properties compared to the other ones.

To investigate the porosity nature and morphology of prepared electrospun fibers (PC and NPC samples), SEM analysis was performed, Fig. 7A–E. All samples showed

obviously the formation of electrospun fiber without agglomeration of nano TiO₂ particles through polymeric matrix. Moreover, the electrospun fibers showed different diameters. All fibers diameter were calculated from the SEM photographs (average value), Table 3. The data exhibited that PC sample has the biggest diameter (F.S = 798 nm), while the NPC3 sample has the smallest one (F.S = 700 nm). Also, the porosity nature of the polymeric matrix was studied using Brunauer–Emmett–Teller (BET) nitrogen adsorption–desorption isotherm. All data were tabulated, Table 3. As shown in Fig. 7 (dVp/W (nm), pore size distribution), the NPC2, NPC3, NPC4 samples showed the highest pore diameter value (24.60 nm) compared to the other ones. This also make the NPC4 sample having another advantage for the electrical properties performance. In contrast, the mean pore diameter value of PC sample (1048 nm) was the highest one compared to the others, confirming that nano TiO₂ filler plays a role in decreasing the pore diameter of the electro spun fibers. Additionally, the mean pore diameter value of NPC2 sample (14.15 nm) was the lowest one. The porous structure of all electrospun fibers electrolytes can increase both of diffusion process of solid state Li-ion [45–49] and accommodate volume changes to keep the structure integrity [50, 51]. To investigate the electrical property of electrospun fibers, all samples (PC, NPC1, NPC2, NPC3 and NPC4) were soaked in a 1 M LTFB to get electrospun fibers electrolytes (PEC, NPEC1, NPEC2, NPEC3, NPEC4).

To study the effect of LTFB salt on the polymeric matrix structure, X-ray diffraction analysis was performed, Fig. 8. As obviously shown, the crystalline peaks of LTFB salt disappeared completely in presence of the polymeric matrix of PC, NPC1, NPC2, NPC3 and NPC4, leading to more amorphous structure for all investigated electrospun fibers. This shows the ability of the polymers matrix to dissociate the salt, and as a result more interactions with lithium ions will be expected. The temperature effect on AC-electrical conductivity of PEC, NPEC1, NPEC2, NPEC3 and NPEC4 was studied in a temperature range of 303–373 K and at a frequency of 100 Hz, Fig. 9A. The figure obviously revealed an increase behavior of the AC-conductivity value with temperature increase for all electrospun fibers electrolytes. This increase behavior follows Arrhenius equation, $\sigma = \sigma_0 \exp(-E_a/RT)$, where R, T, σ and σ_0 are gas constant, temperature, the AC-conductivity and the pre-exponential factor, respectively. Jumping of lithium ions into adjacent vacant sites leads to ionic conductivity value increase. The ions motion in polymer electrolytes can be interpreted in a light of liquid-like mechanism, where the polymer segmental motion can enhance ions movement. Therefore, high temperature induces high segmental motion which helps ion hopping or provides a pathway for faster ionic conductivity [52]. The values of AC-conductivity of all electrospun fibers electrolytes were determined at room temperature,

Fig. 7 SEM photographs of **A** PC; **B** NPC1; **C** NPC2; **D** NPC3 and **E** NPC4

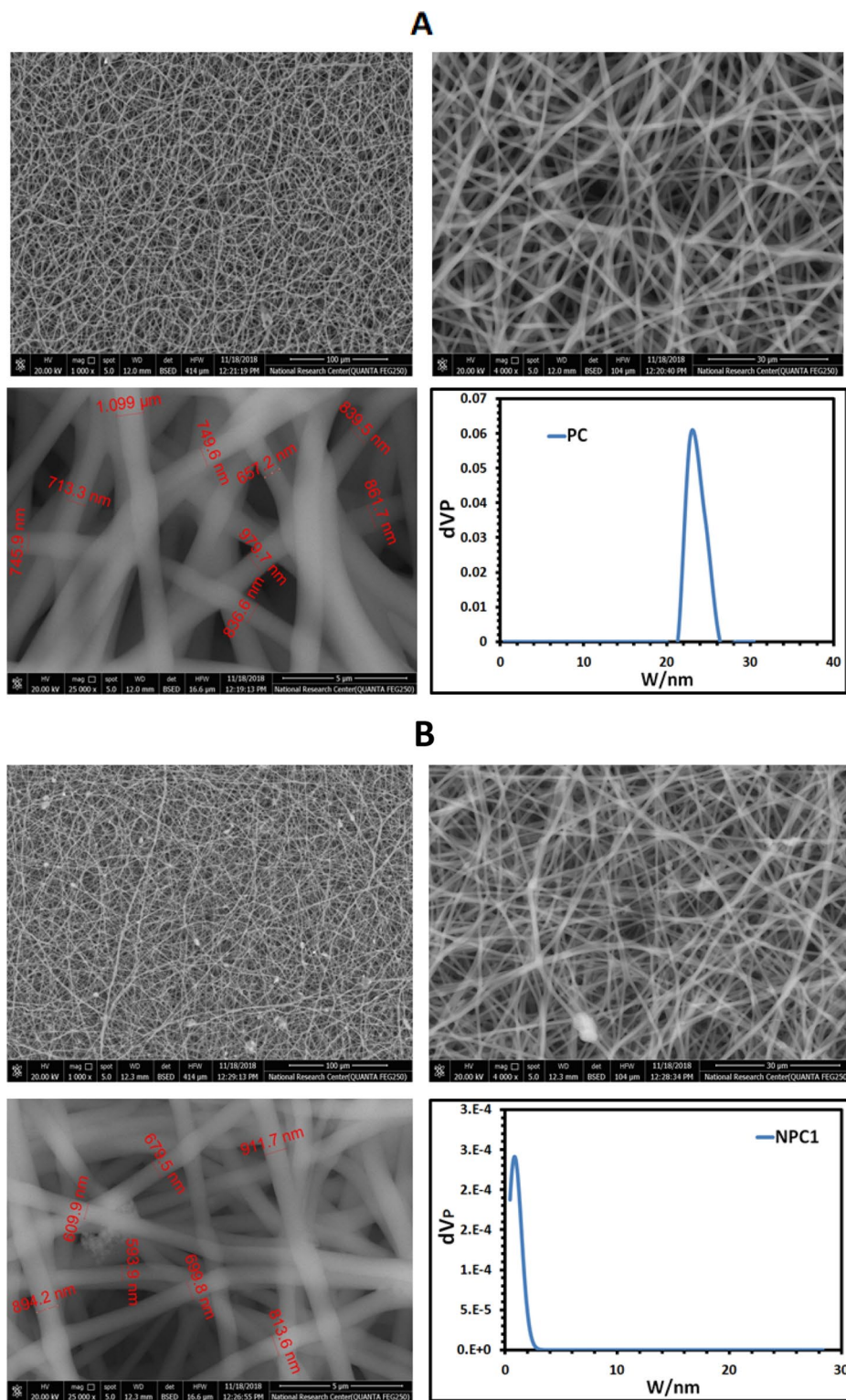
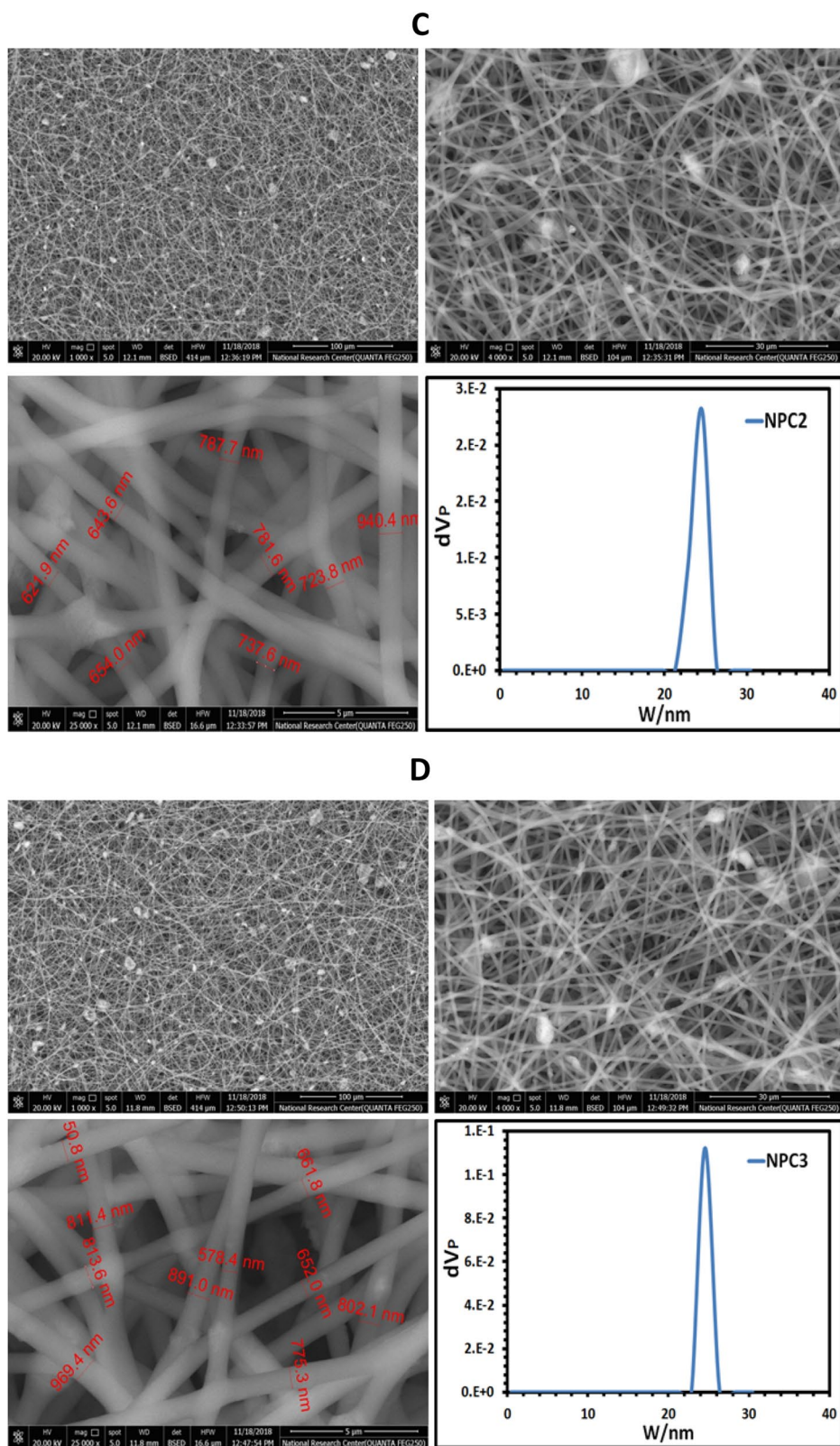


Fig. 9B. From the figure, the NPEC4 sample has the highest ionic conductivity value ($\sigma_{AC} = 1.08 \times 10^{-3} \Omega^{-1} \text{ cm}^{-1}$) compared to the other electrospun fibers electrolytes. This also can be interpreted in vein of the above studied structure characterization of this sample. This sample exhibited

the lowest crystallinity structure, the highest value of both melting and decomposition temperatures and the highest value of pore diameter. All these structural properties support the ions motion through the polymers matrix at low and high temperatures. The others electrospun fibers

Fig. 7 (continued)



electrolytes showed the following AC-conductivity value order: NPEC3; $\sigma_{AC} = 5.03 \times 10^{-4} \Omega^{-1} \text{cm}^{-1} > \text{PEC}$; $\sigma_{AC} = 4.52 \times 10^{-4} \Omega^{-1} \text{cm}^{-1} > \text{NPEC1}$; $\sigma_{AC} = 1.50 \times 10^{-4} \Omega^{-1} \text{cm}^{-1} > \text{N}$

PEC2; $\sigma_{AC} = 1.45 \times 10^{-4} \Omega^{-1} \text{cm}^{-1}$. These results exhibit that TiO_2 addition creates favorable pathways for the free lithium ions through Lewis acid–base interactions between different

Fig. 7 (continued)

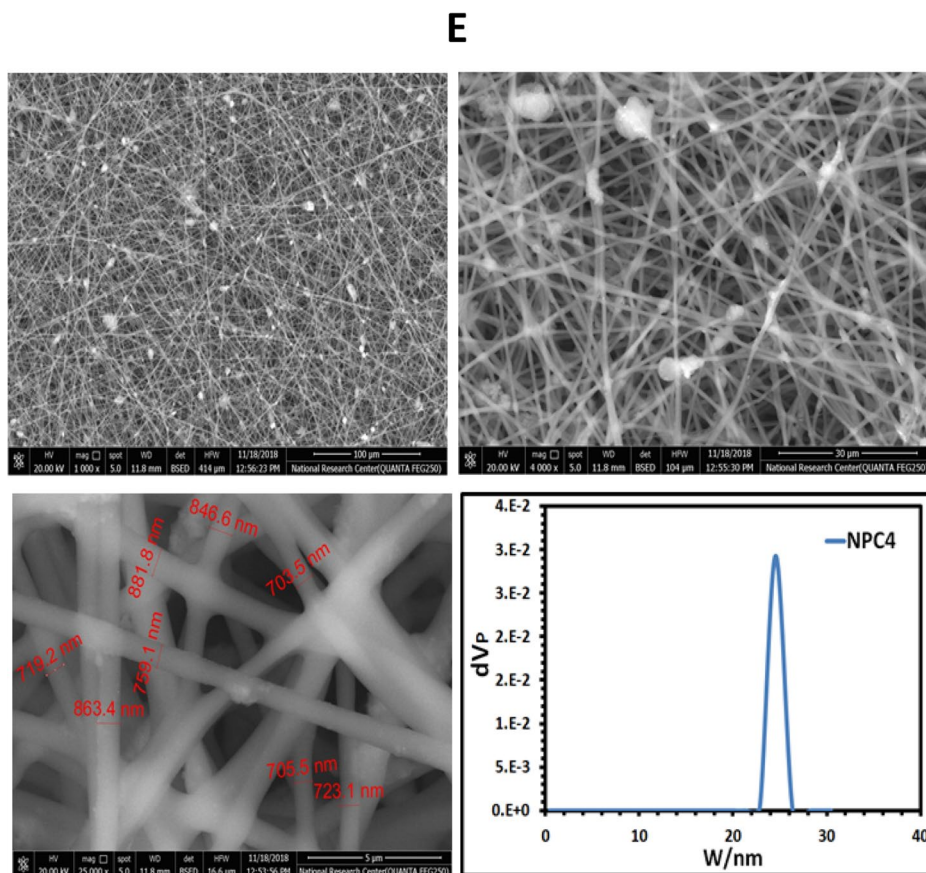


Table 3 Parameters values of N₂ adsorption/desorption isotherms and NLDFT/GCMC pore size distribution analysis of PC, NPC1, NPC2, NPC3 and NPC4

Sample	Fiber diameter (nm)	Total pore volume (cm ³ /g)	Mean pore diameter (nm)	W, peak (Area) (nm)	Vp (cm ³ /g)
PC	798	9.50 × 10 ⁻²	1048	22.80	9.60 × 10 ⁻²
NPC1	743	2.65 × 10 ⁻²	46.50	0.44	4.21 × 10 ⁻³
NPC2	736	3.04 × 10 ⁻²	14.15	24.60	3.25 × 10 ⁻²
NPC3	700	9.60 × 10 ⁻²	155.30	24.60	11 × 10 ⁻²
NPC4	775	2.85 × 10 ⁻²	42.30	24.60	2.95 × 10 ⁻²

species in the polymers matrix [53]. Moreover, the activation energy (E_a) values of all electrospun fibers electrolytes were also calculated using the Arrhenius model. The values of activation energy were represented in Fig. 9C. These values reflects the energy related to the defect formation and the ion migration process. Additionally, activation energy value gives an indication for the suitable environment and the ion migration conditions for smoother ion transport. The high activation energy value can also be attributed to the high energy of ion migration [54, 55]. Figure 9C showed that NPE4 has the lowest activation energy value ($E_a = 0.12$ eV)

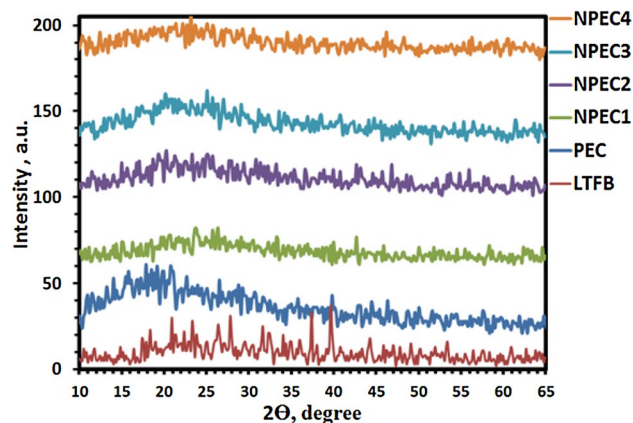


Fig. 8 X-ray diffraction patterns of LTFB, PEC, NPE1, NPE2, NPE3 and NPE4

compared to the others electrospun fibers electrolytes, which showed the following order: NPE1; $E_a = 0.31$ eV > NPE2; $E_a = 0.30$ > NPE3 = PEC; $E_a = 0.18$ eV. The lowest activation energy value of NPE4 comes in a good matching with the same electrospun fiber electrolyte of the highest conductivity value, stating that activation energy of the free ions determines ionic conductivity value, and the smaller the activation energy value, the smoother the cation migration [56].

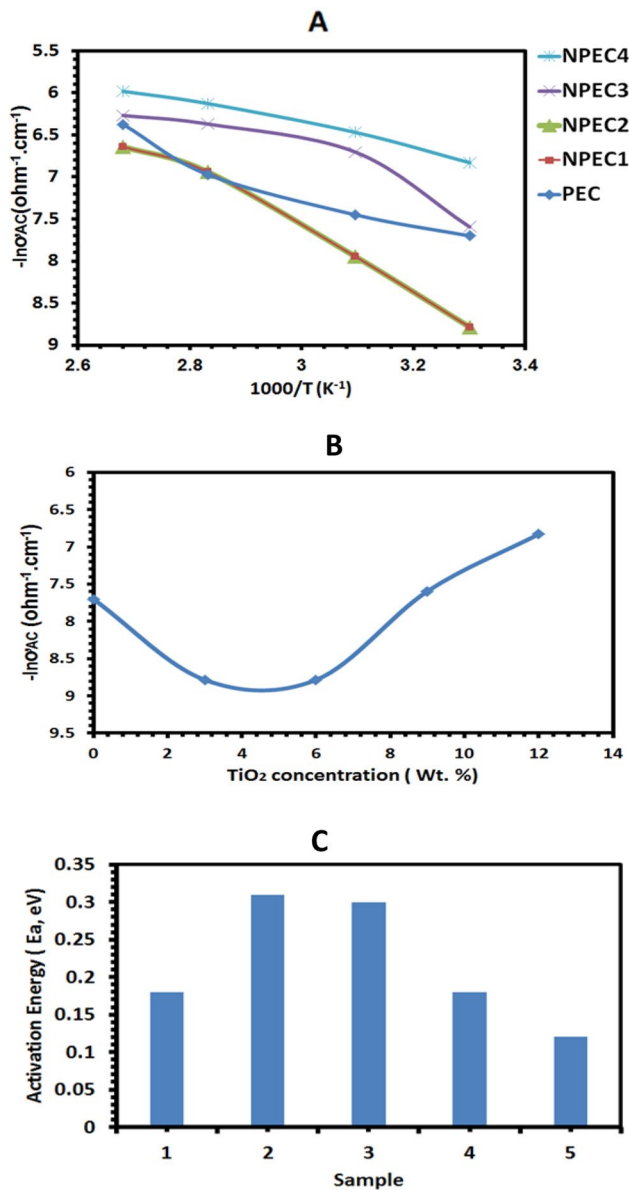


Fig. 9 **A** Temperature dependence of AC-conductivity (at 100 Hz frequency), **B** nano filler (TiO₂) concentration dependence of AC-conductivity (at room temperature, 303 K) and **C** Activation energy values for PEC, NPEC1, NPEC2, NPEC3 and NPEC4

Figure 10 showed the frequency dependence (from 100 Hz to 1 MHz) of AC-conductivity for PEC, NPEC1, NPEC2, NPEC3 and NPEC4 at room temperature (303 K). The figure showed an increase behavior of AC-conductivity value with frequency. Also, the NPEC4 sample exhibited the highest AC-conductivity values compared to the others at all different frequencies values. According to the above structure and properties results of the investigated electrospun fiber electrolytes, the NPEC4 sample is the best one exhibiting good ionic conductivity value at room temperature with a good thermal stability behavior. More studies of the electrical

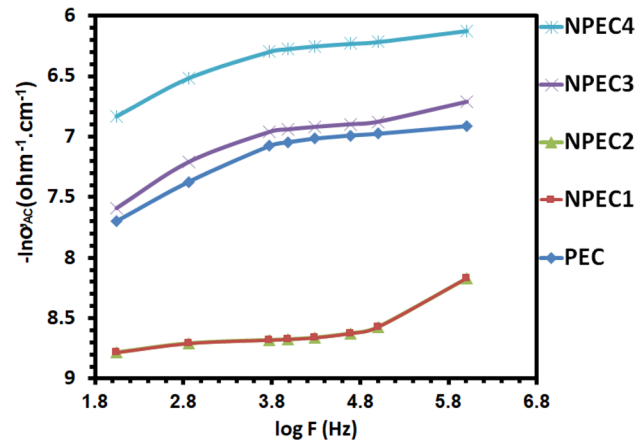


Fig. 10 Frequency dependence of AC-conductivity for PEC, NPEC1, NPEC2, NPEC3 and NPEC4 at room temperature (303 K)

properties will be discussed for NPEC4 sample to investigate its ability as a solid electrolyte for lithium ion batteries application. Figure 11A shows the temperature effect on AC-conductivity at different frequencies (100 Hz–1 MHz) for NPEC4 sample. The AC-conductivity increases with temperature increasing, and also with frequency increasing as well. The activation energy values, at different frequencies, were calculated using the Arrhenius model. Figure 11B shows the frequency effect on activation energy for NPEC4 sample. The figure exhibited a decrease behavior of activation energy values with frequency increasing. This can be attributed to the enhanced lithium ion motion with frequency increase [19]. Also, the frequency dependence of AC-conductivity at different temperatures for NPEC4 sample was also studied, Fig. 11C. The figure showed an increase behavior in two ranges; the first was from 100 Hz to 1 kHz, and the second from 1 kHz to 1 MHz. Effect of Temperature and frequency on dielectric constant, at different frequencies (100 Hz to 1 MHz) and temperatures (303 to 373 K), was investigated for NPEC4 sample, Fig. 12A, B. Figure 12A showed an increase of dielectric constant value with temperature at different frequencies. This behavior can be interpreted in a light of viscosity decrease [57] of the polymers matrix. Moreover, crystalline or semi-crystalline phases of NPEC4 sample may dissolve, at high temperatures, in the amorphous phase [58]. Figure 12B showed that dielectric constant decreases with frequency increasing at different temperatures, which may be attributed to the interface charge accumulation that causes an ionic medium polarization process, which form a space charge region at the interface of electrode-electrolyte [59–65]. Also, From the figure, The NPEC4 sample showed dielectric constant (ϵ') value equals 5,656,154 at room temperature (303 K) and 100 Hz.

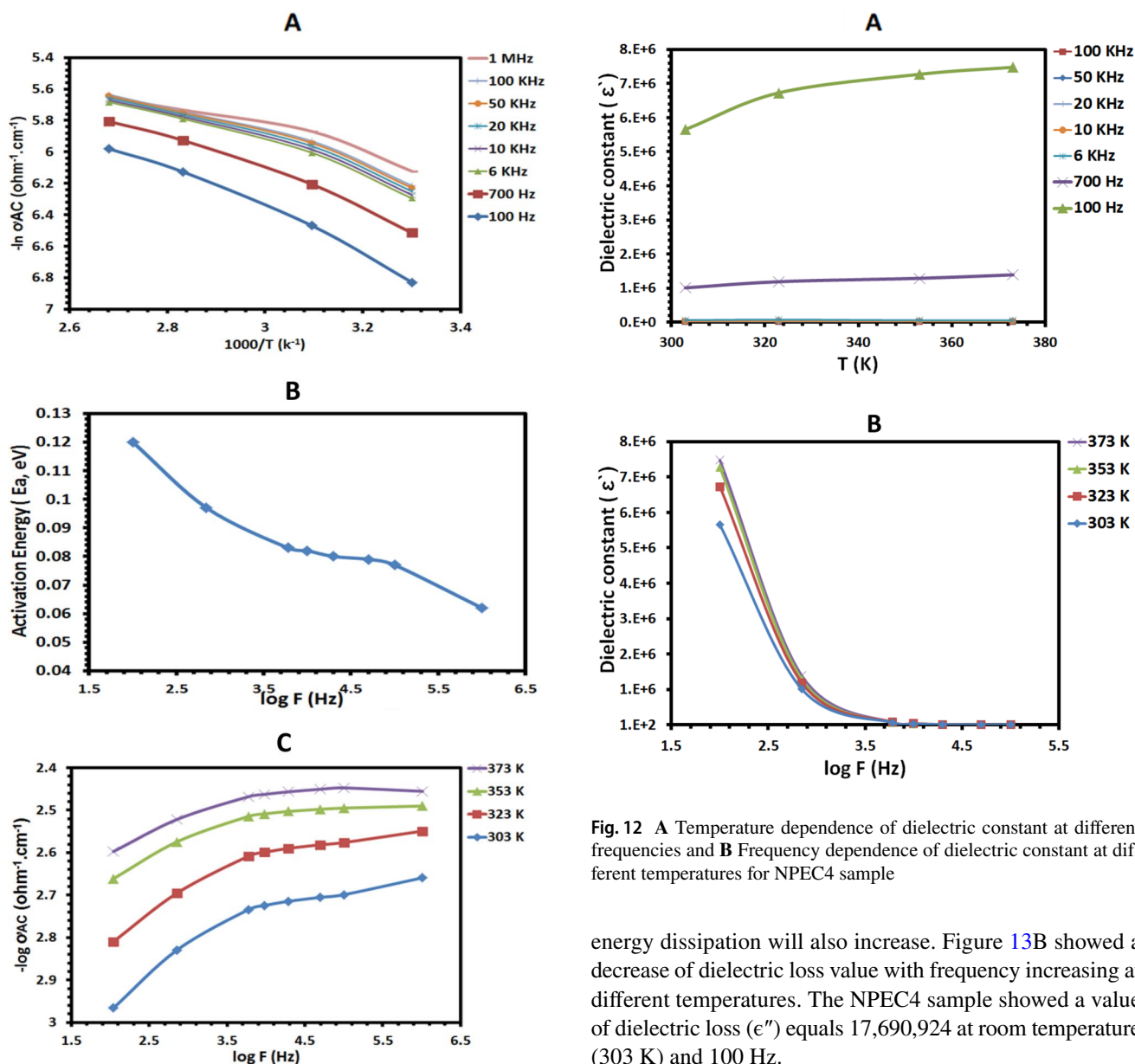


Fig. 11 A Temperature dependence of AC-conductivity at different frequencies, B Frequency dependence of activation energy and C Frequency dependence of AC-conductivity at different temperatures for NPEC4 sample

The temperature and frequency dependence of dielectric loss at different frequencies (100 Hz to 1 MHz) and temperatures (303 to 373 K), was also investigated for NPEC4, Fig. 13A, B. Figure 13A exhibited an increase of dielectric loss value with temperature increasing at different frequencies. This behavior may be attributed to the relaxation process of the dipole molecules in presence of relaxation time resulting drop. This process exerts a dielectric loss double effect. The dipoles friction will increase and as a result,

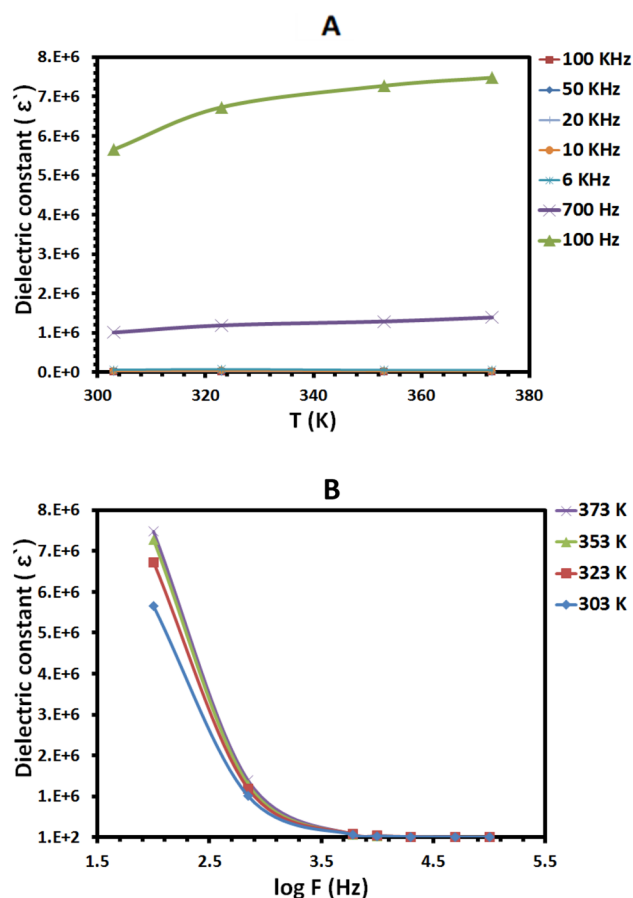


Fig. 12 A Temperature dependence of dielectric constant at different frequencies and B Frequency dependence of dielectric constant at different temperatures for NPEC4 sample

energy dissipation will also increase. Figure 13B showed a decrease of dielectric loss value with frequency increasing at different temperatures. The NPEC4 sample showed a value of dielectric loss (ϵ'') equals 17,690,924 at room temperature (303 K) and 100 Hz.

To further study the dielectric relaxation behavior, dielectric modulus was also investigated for NPEC4 sample. Both of real and imaginary parts (M' , M'') of dielectric modulus, at different temperatures, were represented in Fig. 14A, B. As obviously seen, the relaxation peaks are absent. Additionally, an increase values were observed in the high frequency range. Also, the sample exhibited a long tail before the zero end for all temperatures of low frequency range. This long tail represents the electrical double layer suppression effect at electrode–electrolyte area [66], which can be attributed to the high electrode capacity value of the polymer electrolytes [67].

Figure 15 shows a complex impedance of NPEC4 sample at different temperatures. The figure represented a spectrum consists of a semicircular part and a spike. This

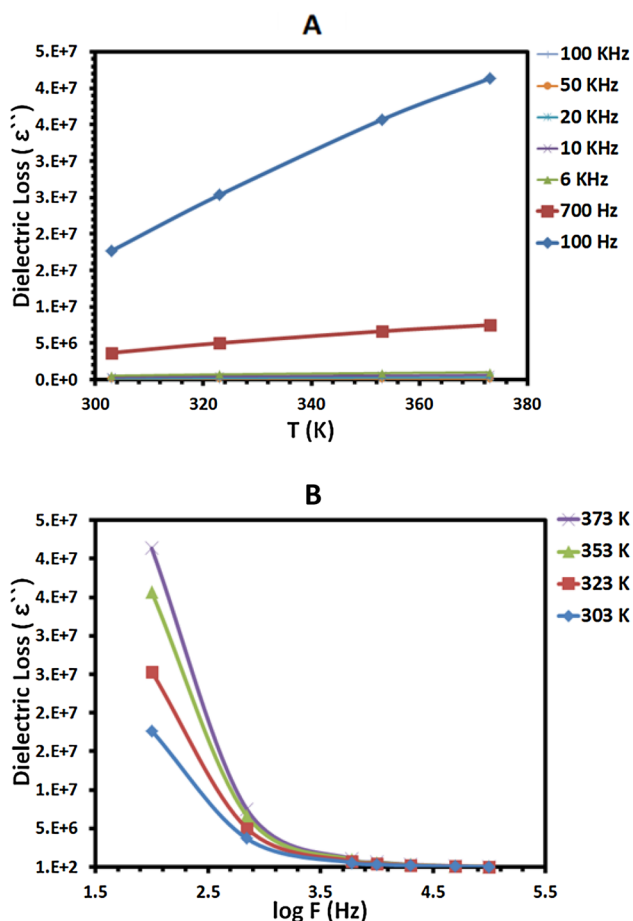


Fig. 13 **A** Temperature dependence of dielectric loss at different frequencies and **B** Frequency dependence of dielectric loss at different temperatures for NPEC4 sample

spike reflects the ionic conduction nature and blocking double layer capacitance. The semicircular part at high frequencies can be attributed to the conduction process increase when frequency increases [68]. The equivalent circuit was also included in Fig. 15, where R1 is the bulk resistance of the electrolyte, CPE1 is the bulk capacity of the electrolyte and CPE2 is a capacity of bulk electrode–electrolyte interface. Figure 16 showed that bulk ionic conductivity value increases with temperature increasing, exhibiting the following order at different temperatures: $\sigma_b = 2.16 \times 10^{-3} \Omega^{-1} \text{ cm}^{-1}$ at 303 K $< \sigma_b = 2.78 \times 10^{-3} \Omega^{-1} \text{ cm}^{-1}$ at 323 K $< \sigma_b = 3.29 \times 10^{-3} \Omega^{-1} \text{ cm}^{-1}$ at 353 K $< \sigma_b = 3.63 \times 10^{-3} \Omega^{-1} \text{ cm}^{-1}$ at 373 K.

Comparison of electrical properties for electrospun fiber nano composite electrolyte (NPEC4) sample with previous studied similar electrolyte systems was performed, Table 4.

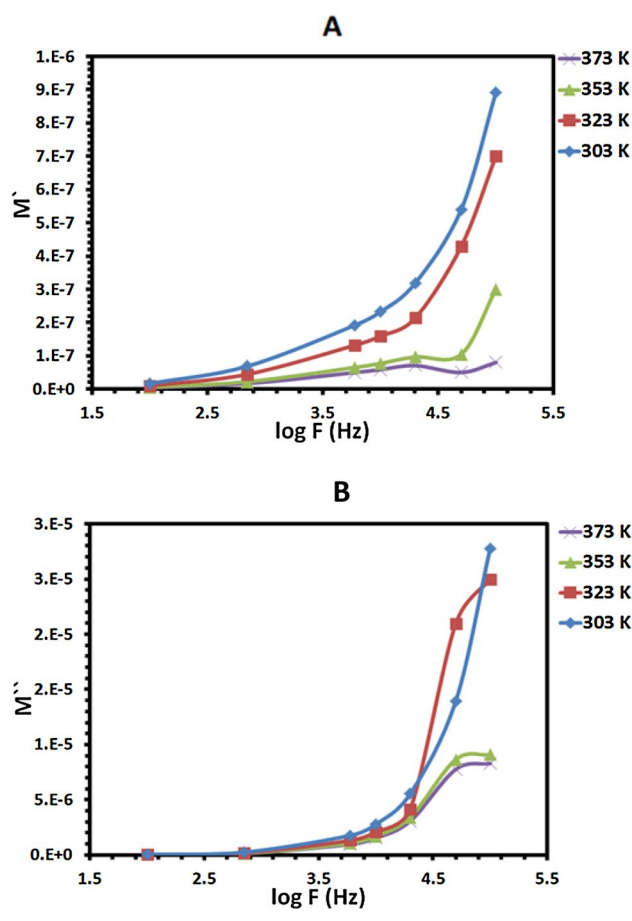


Fig. 14 Frequency dependence of Modulus; **A** M' and **B** M'' at different temperatures for NPEC4 sample

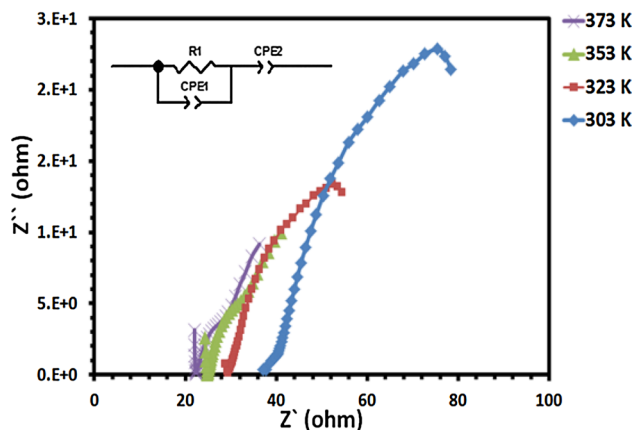


Fig. 15 Complex impedance spectra for NPEC4 sample at different temperatures

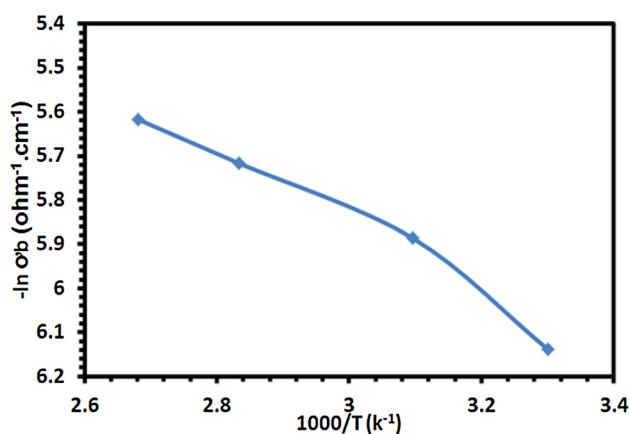


Fig. 16 Temperature dependence of bulk conductivity for NPEC4 sample

The table showed good values of conductivity, dielectric constant and dielectric loss of this sample compared to literature ones.

From all the above studied electrical properties results, in addition to those of the comparison ones, we can conclude that this electrospun fiber electrolyte can be considered as a promised solid electrolyte for lithium-ion batteries application.

4 Conclusions

As a new methodology, electrospun fibers nano composites solid electrolytes containing three different polymers of PMMA, PVDF-co-HFP and PEO, in and without presence of nano TiO₂ filler were successfully synthesized using electrospinning technique. The complete dissolution of LTFB salt into polymers matrix was confirmed by XRD analysis. SEM showed the good dispersion of nano TiO₂ filler within the three polymers matrix, in addition to the formation of fibers. The NPEC4 sample showed the optimized structural properties, which support the improved electrical properties. This sample exhibited high melting ($T_m = 319$ °C) and decomposition ($T_d = 411$ °C) temperatures compared to the other ones. At the same time, this sample showed the lowest crystallinity structure, which was confirmed from X-ray diffraction. Moreover, a high value of the pore diameter was achieved for the same sample with fiber diameter equals 775 nm. Good electrical properties were observed for this sample, such as the highest ionic conductivity ($\sigma_{AC} = 1.08 \times 10^{-3} \Omega^{-1} \text{cm}^{-1}$ at room temperature), high dielectric constant and loss (5,656,154 and 17,690,924, respectively, at room temperature (303 K) and 100 Hz) and high bulk ionic conductivity value ($\sigma_b = 2.16 \times 10^{-3} \Omega^{-1} \text{cm}^{-1}$ at room temperature (303 K)). All the studied electrical properties results and those of the comparison ones exhibited the ability of this electrospun fiber nano composite electrolyte to be used

Table 4 Comparison of electrical properties for electrospun fiber nano composite electrolyte (NPEC4) sample with previous studied similar electrolyte systems

System	Dielectric constant (ϵ'), at room temperature and 100 Hz	Dielectric Loss (ϵ''), at room temperature and 100 Hz	Ionic conductivity (σ_{AC}), ohm ⁻¹ cm ⁻¹ , at room temperature and 100 Hz	References
Electrospun nano fiber (PMMA/PVdF-co-HFP/PEO/TiO ₂)/LTFB	5,656,154	17,690,924	1.08×10^{-3}	This study
Polymethylmethacrylate/LiCF ₃ SO ₃ /montmorillonite	834	37,500	2.09×10^{-6}	[19]
PEO/LiClO ₄ /nano Al ₂ O ₃	2.21×10^6	7.42×10^6	8.30×10^{-5}	[39]
PVdF-co-HFP/PVAc/LiPF ₆ /nano ZnO	2.00×10^3	19,450	3.69×10^{-4}	[41]
PVdF-co-HFP/LiCF ₃ SO ₃ /nano MgO	450	11,750	8.78×10^{-5}	[52]
PEO/LiClO ₄ /nano LiAlO ₂	1.22×10^6	1.05×10^7	9.76×10^{-5}	[69]
PEO/LiClO ₄ /ZnO	8.58×10^5	6.30×10^6	6.33×10^{-5}	[70]
PVdF-co-HFP/PVAc/LiCF ₃ SO ₃ /nano LiAlO ₂ (gel electrolyte)	1.00×10^5	79,432	4.98×10^{-3}	[71]
PVdF-co-HFP/PVAc/LiClO ₄ /nano Citric acid	–	–	8.00×10^{-4}	[72]
PVdF/Clay/LiPF ₆ (gel electrolyte)	–	–	3.08×10^{-3}	[73]

as a promised solid electrolyte for lithium-ion batteries application.

Acknowledgements The first and corresponding author of this paper wish to extend his sincere gratitude to the Deanship of Scientific Research at the Islamic University of Madinah for the support provided to the Post-Publishing Program 1.

Author contributions Emad M. Masoud prepared Figures and wrote the main manuscript. Other authors reviewed the manuscript.

Funding The authors have not disclosed any funding.

Declarations

Conflict of interest The authors declare that they have no conflict of interest.

References

- Z. Peng, Q. Jiang, P. Peng, F.-F. Li, NH_3 -activated fullerene derivative hierarchical microstructures to porous $\text{Fe}_3\text{O}_4/\text{N-C}$ for oxygen reduction reaction and Zn-air battery. *Eng. Sci.* **14**, 27–38 (2021)
- Y. Lv, L. Zhu, X. Haoxiang, L. Yang, Z. Liu, D. Cheng, X. Cao, J. Yun, D. Cao, Core/shell template-derived Co, N-doped carbon bifunctional electrocatalysts for rechargeable Zn-air battery. *Eng. Sci.* **7**, 26–37 (2019)
- X. Hu, H. Wu, S. Liu, S. Gong, Y. Du, X. Li, X. Lu, J. Qu, Fabrication of organic shape-stabilized phase change material and its energy storage applications. *Eng. Sci.* **17**, 1–27 (2022)
- C. Hou, B. Wang, V. Murugadoss, S. Vupputuri, Y. Chao, Z. Guo, C. Wang, D. Wei, Recent advances in Co_3O_4 as anode materials for high-performance lithium-ion batteries. *Eng. Sci.* **11**, 19–30 (2020)
- L. Xiang, H. Liu, V. Murugadoss, I. Seok, J. Huang, J.E. Ryu, Z. Guo, Polyethylene glycol/carbon black shape-stable phase change composites for peak load regulating of electric power system and corresponding thermal energy storage. *Eng. Sci.* **9**, 25–34 (2020)
- S.S. Patil, T.S. Bhat, A.M. Teli, S.A. Beknalkar, S.B. Dhavale, M.M. Faras, M.M. Karanjkar, P.S. Patil, Hybrid solid state supercapacitors (HSSC's) for high energy & power density: an overview. *Eng. Sci.* **12**, 38–51 (2020)
- Y. Wang, Y. Liu, C. Wang, H. Liu, J. Zhang, J. Lin, J. Fan, T. Ding, J.E. Ryu, Z. Guo, Significantly enhanced ultrathin NiCo-based MOF nanosheet electrodes hybridized with $\text{Ti}_3\text{C}_2\text{Tx}$ MXene for high performance asymmetric supercapacitor. *Eng. Sci.* **9**, 50–59 (2020)
- Z. Wang, S. He, V. Nguyen, K.E. Riley, Ionic liquids as “green solvent and/or electrolyte” for energy interface. *Eng. Sci.* **11**, 3–18 (2020)
- E.M. Masoud, S. Indris, Block-shaped pure and doped $\text{Li}_4\text{Ti}_5\text{O}_{12}$ containing a high content of a Li_2TiO_3 dual phase: an anode with excellent cycle life for high rate performance lithium-ion batteries. *RSC Adv.* **5**, 108058–108066 (2015)
- E.M. Masoud, Nano $\alpha\text{-Fe}_2\text{O}_3$ synthesized using EDTA-aqueous solution simple and novel method: improved capacity retention at 1 C rate as anode for high rate performance of lithium-ion batteries. *Ionics* **27**, 2847–2855 (2021)
- E.M. Masoud, Mesoporous nano nickel oxide: anode with good initial discharge capacity and efficiency in lithium ion batteries at 1 C rate. *J. Alloys Compd.* **585**, 357–361 (2014)
- E.M. Masoud, Improved initial discharge capacity of nanostructured Ni-Co spinel ferrite as anode in lithium ion batteries at 1 C rate. *Solid State Ion.* **253**, 247–252 (2013)
- C. Hou, J. Hou, H. Zhang, Y. Ma, X. He, W. Geng, Q. Zhang, Facile synthesis of $\text{LiMn}_{0.75}\text{Fe}_{0.25}\text{PO}_4/\text{C}$ nanocomposite cathode materials of lithium-ion batteries through microwave sintering. *Eng. Sci.* **11**, 36–43 (2020)
- H. Tong, Q. Zhou, B. Zhang, X. Wang, Y. Yao, Z. Ding, H. Chen, J.C. Zheng, W. Yu, A novel core-shell structured nickel-rich layered cathode material for high-energy lithium-ion batteries. *Eng. Sci.* **8**, 25–32 (2019)
- Y. Li, G. Xu, Y. Yao, L. Xue, M. Yanilmaz, H. Lee, X. Zhang, Coaxial electrospun Si/C-C core-shell composite nanofibers as binder-free anodes for lithium-ion batteries. *Solid State Ion.* **258**, 67–73 (2014)
- H. Lee, M. Yanilmaz, O. Toprakci, K. Fu, X. Zhang, A review of recent developments in membrane separators for rechargeable lithium-ion batteries. *Energy Environ. Sci.* **7**, 3857–3886 (2014)
- D. Andersson, P. Carlsson, D. Engberg, L.M. Torell, L. Borjesson, R.L. McGreevy, W.S. Howells, Modelling of segmental dynamics in polymer electrolyte PPO- LiClO_4 , by surface fitting of quasi-elastic neutron scattering data. *Physica B* **266**, 126–130 (1999)
- Y. Tominaga, T. Mizumo, H. Ohno, Ionic conductivity of PPO-sulfonamide salt hybrids and their network polymers. *Polym. Adv. Technol.* **11**, 524–528 (2000)
- E.M. Masoud, Montmorillonite incorporated polymethylmethacrylate matrix containing lithium trifluoromethanesulphonate (LTF) salt: thermally stable polymer nanocomposite electrolyte for lithium-ion batteries application. *Ionics* **25**, 2645–2656 (2019)
- E.A. Baroncini, D.M. Rousseau, C.A. Strekis, J.F. Stanzione, Optimizing conductivity and cationic transport in cross linked solid polymer electrolytes. *Solid State Ion.* **345**, 115161 (2020)
- N.P. Young, D. Devaux, R. Khurana, G.W. Coates, N.P. Balsara, Investigating polypropylene-poly (ethylene oxide)-polypropylene triblock copolymers as solid polymer electrolytes for lithium batteries. *Solid State Ion.* **263**, 87–94 (2014)
- H.R. Allcock, M.E. Napierala, D.L. Olmeijer, C.G. Cameron, S.E. Kuharcik, C.S. Reed, S.J.M. O'Connor, New macromolecules for solid polymeric electrolytes. *Electrochim. Acta* **43**, 1145–1150 (1998)
- T. Eriksson, A. Mace, Y. Manabe, M. Yoshizawa-Fujita, Y. Inokuma, D. Brandell, J. Mindemark, Polyketones as host materials for solid polymer electrolytes. *J. Electrochem. Soc.* **167**, 070537 (2020)
- G. Tian, Z. Zhao, T. Zinkevich, K. Elies, F. Scheiba, H. Ehrenberg, A crosslinked polyethyleneglycol solid electrolyte dissolving lithium bis (trifluoromethylsulfonyl) imide for rechargeable lithium batteries. *Chemsuschem* **12**, 4708–4718 (2019)
- S. Wang, K. Min, Solid polymer electrolytes of blends of polyurethane and polyether modified polysiloxane and their ionic conductivity. *Polymer* **51**, 2621–2628 (2010)
- J.C. Barbosa, J.P. Dias, S. Lanceros-Méndez, C.M. Costa, Recent advances in poly (vinylidene fluoride) and its copolymers for lithium-ion battery separators. *Membranes* **8**, 45 (2018)
- V.O. Yarmolenko, V.A. Yudina, K.G. Khatmullina, Nanocomposite polymer electrolytes for the lithium power sources. *Russ. J. Electrochem.* **54**, 325–343 (2018)
- S. Sathish, B.C. Shekar, Preparation and characterization of nano scale PMMA thin films. *Indian J. Pure Appl. Phys.* **52**, 64–67 (2014)
- S.A.M. Noor, P.M. Bayley, M. Forsyth, D.R. MacFarlane, Ionogels based on ionic liquids as potential highly conductive solid state electrolytes. *Electrochim. Acta* **91**, 219–226 (2013)
- T.I.S. Carvalho, *Development of Ion Jelly Thin Films for Electrochemical Devices* (Faculdade de Ciência e Tecnologia da Universidade Nova de Lisboa, Lisboa, 2013)

31. X. Zai-Lai, A. Jeličić, F.-P. Wang, P. Rabu, A. Friedrich, Transparent, flexible, and paramagnetic ionogels based on PMMA and the iron-based ionic liquid 1-butyl-3-methylimidazolium tetrachloroferrate (III)[Bmim][FeCl₄]. *J. Mater. Chem.* **20**, 9543–9549 (2010)
32. K. Lunstroot, K. Driesen, P. Nockemann, L. Viau, P.H. Mutin, A. Vioux, K. Binnemans, Ionic liquid as plasticizer for europium (III)-doped luminescent poly (methyl methacrylate) films. *Phys. Chem. Chem. Phys.* **12**, 1879–1885 (2010)
33. C.K. Park, A. Kakirde, W. Ebner, V. Manivannan, C. Chai, D.J. Ihm, Y.J. Shim, High temperature stable lithium-ion polymer battery. *J. Power Sour.* **97**, 775 (2001)
34. Y. Wang, J.T. Sejdic, R. Steiner, Polymer gel electrolyte supported with microporous polyolefin membranes for lithium ion polymer battery. *Solid State Ion.* **148**, 443 (2002)
35. D. Saikia, A. Kumar, Ionic conduction in P (VdF-HFP)/PVdF-(PC+DEC)-LiClO₄ polymer gel electrolytes. *Electrochim. Acta* **49**, 2581 (2004)
36. Z. Xue, D. He, X. Xie, Poly(ethylene oxide)-based electrolytes for lithium-ion batteries. *J. Mater. Chem. A* **3**(38), 19218–19253 (2015)
37. J. Mindemark, M.J. Lacey, T. Bowden, D. Brandell, Beyond PEO—alternative host materials for Li⁺-conducting solid polymer electrolytes. *Prog. Polym. Sci.* **81**, 114–143 (2018)
38. A. Manthiram, X. Yu, S. Wang, Lithium battery chemistries enabled by solid-state electrolytes. *Nat. Rev. Mater.* **2**(4), 16103 (2017)
39. E.M. Masoud, A.-A. Elbellihi, W.A. Bayoumy, M.A. Mousa, Organic–inorganic composite polymer electrolyte based on PEO–LiClO₄ and nano-Al₂O₃ filler for lithium polymer batteries: Dielectric and transport properties. *J. Alloys Compd.* **575**, 223–228 (2013)
40. J. Zhou, P.S. Fedkiw, Ionic conductivity of composite electrolytes based on oligo (ethylene oxide) and fumed oxides. *Solid State Ion.* **166**, 275–293 (2004)
41. E.M. Masoud, M.E. Hassan, S.E. Wahdaan, S.R. Elsayed, S.A. Elsayed, Gel P (VdF/HFP) /PVAc/lithium hexafluorophosphate composite electrolyte containing nano ZnO filler for lithium ion batteries application: effect of nano filler concentration on structure, thermal stability and transport properties. *Polym. Test.* **56**, 277–286 (2016)
42. M. Moskwiak, I. Giska, R. Borkowska, A. Zalewska, M. Marczewski, H. Marczewska, W. Wiecek, Physico-and electrochemistry of composite electrolytes based on PEODME–LiTFSI with TiO₂. *J. Power Sour.* **159**, 443–448 (2006)
43. L. Sannier, A. Zalewska, W. Wiecek, M. Marczewski, H. Marczewska, Impact of “Super Acid” like filler on the properties of a PEGDME/LiClO₄ system. *Electrochim. Acta* **52**, 5685–5689 (2007)
44. M. Stolarska, L. Niedzicki, R. Borkowska, A. Zalewska, W. Wiecek, Structure, transport properties and interfacial stability of PVdF/HFP electrolytes containing modified inorganic filler. *Electrochim. Acta* **53**, 1512–1517 (2007)
45. B.Q. Liu, Q.F. Li, B. Zhang, Y.L. Cui, H.F. Chen, G.N. Chen, D.P. Tang, Synthesis of patterned nanogold and mesoporous CoFe₂O₄ nanoparticle assemblies and their application in clinical immunoassays. *Nanoscale* **3**, 2220 (2011)
46. D.W. Liu, B.B. Garcia, Q.F. Zhang, Q. Guo, Y.H. Zhang, S. Sepehri, G.Z. Cao, Mesoporous hydrous manganese dioxide nanowall arrays with large lithium ion energy storage capacities. *Adv. Funct. Mater.* **19**, 1015 (2009)
47. C.M. Park, J.K. Jeon, Porous structured SnSb/C nanocomposites for Li-ion battery anodes. *Chem. Commun.* **47**, 2122 (2011)
48. X.W. Lou, D. Deng, J.Y. Lee, L.A. Archer, Preparation of SnO₂/Carbon composite hollow spheres and their lithium storage properties. *Chem. Mater.* **20**, 6562 (2008)
49. H.S. Zhou, D.L. Li, M. Hibino, I. Honma, A self-ordered, crystalline–glass, mesoporous nanocomposite for use as a lithium-based storage device with both high power and high energy densities. *Angew. Chem. Int. Ed.* **44**, 797 (2005)
50. S.M. Yuan, J.X. Li, L.T. Yang, L.W. Su, L. Liu, Z. Zhou, Preparation and lithium storage performances of mesoporous Fe₃O₄@C microcapsules. *Appl. Mater. Interfaces* **3**, 705 (2011)
51. C. Burda, X.B. Chen, R. Narayanan, M.A. El-sayed, Chemistry and properties of nanocrystals of different shapes. *Chem. Rev.* **105**, 1025 (2005)
52. E.M. Masoud, A.-A. El-Bellih, W.A. Bayoumy, E.A. Mohamed, Polymer composite containing nano magnesium oxide filler and lithiumtriflate salt: an efficient polymer electrolyte for lithium ion batteries application. *J. Mol. Liq.* **260C**, 237–244 (2018)
53. F. Croce, G.B. Appetecchi, L. Persi, B. Scrosati, Nanocomposite polymer electrolytes for lithium batteries. *Nature* **394**, 456–458 (1998)
54. F. Latif, M. Aziz, N. Katun, M.Z. Yahya, The role and impact of rubber in poly (methyl methacrylate)/lithium triflate electrolyte. *J. Power Sour.* **159**, 1401–1404 (2006)
55. A.A. Mohamad, N.S. Mohamed, M.Z. Yahya, R. Othman, S. Ramesh, Y. Alias, A.K. Arof, Ionic conductivity studies of poly (vinyl alcohol) alkaline solid polymer electrolyte and its use in nickel–zinc cells. *Solid State Ion.* **177**, 156–171 (2003)
56. A. Arya, A.L. Sharma, Optimization of salt concentration and explanation of two peak percolation in blend solid polymer nanocomposite films. *J. Solid State Electrochem.* **22**, 2725–2745 (2018)
57. B.V.R. Chodari, W. Wang (eds.), *Solid State Ionics: Materials and Devices.* (World Scientific, Singapore, 2000)
58. L. Hu, Z. Tang, Z. Zhang, New composite polymer electrolyte comprising mesoporous lithium aluminate nanosheets and PEO/LiClO₄. *J. Power Sour.* **166**, 226–232 (2007)
59. S. Anderson, R.L. Bohon, D.D. Kimpton, Infrared spectra and atomic arrangement in fused boron oxide and soda borate glasses. *J. Am. Ceram. Soc.* **38**, 370–377 (1955)
60. S. Ren, Z. Chen, T. Yan, F. Han, X. Kuang, L. Fang, L. Liu, High temperature dielectrics and defect characteristic of (Nb, Mn, Zr) modified 0.4 (Ba_{0.8}Ca_{0.2}) TiO_{3-0.6} Bi (Mg_{0.5}Ti_{0.5}) O₃ ceramics. *J. Phys. Chem. Solids* **118**, 99–108 (2018)
61. F. Han, S. Ren, J. Deng, T. Yan, X. Ma, B. Peng, L. Liu, Dielectric response mechanism and suppressing high-frequency dielectric loss in Y₂O₃ grafted CaCu₃Ti₄O₁₂ ceramics. *J. Mater. Sci.: Mater. Electron.* **28**, 17378–17387 (2017)
62. J. Deng, L. Liu, X. Sun, S. Liu, T. Yan, L. Fang, B. Elouadi, Dielectric relaxation behavior and mechanism of Y₂/3Cu₃Ti₄O₁₂ ceramic. *Mater. Res. Bull.* **88**, 320–329 (2017)
63. F. Han, J. Deng, X. Liu, T. Yan, S. Ren, X. Ma, S. Liu, B. Peng, L. Liu, High-temperature dielectric and relaxation behavior of Yb-doped Bi_{0.5}Na_{0.5}TiO₃ ceramics. *Ceram. Int.* **43**, 5564–5573 (2017)
64. X. Sun, J. Deng, S. Liu, T. Yan, B. Peng, W. Jia, Z. Mei, L. Fang, L. Liu, Grain boundary defect compensation in Ti-doped BaFe_{0.5}Nb_{0.5}O₃ ceramics. *Appl. Phys. A* **122**(864), 1–8 (2016)
65. S. Liu, X. Sun, B. Peng, H. Su, Z. Mei, Y. Huang, J. Deng, C. Su, L. Fang, L. Liu, Dielectric properties and defect mechanisms of (1-x) Ba (Fe_{0.5}Nb_{0.5}) O_{3-x} BiYbO₃ ceramics. *J. Electroceram.* **37**, 137–144 (2016)
66. M.C.R. Shastri, K.J. Rao, Ac conductivity and dielectric relaxation studies in AgI-based fast ion conducting glasses. *Solid State Ion.* **44**, 187–198 (1991)
67. S.A. Suthanthiraj, D.J. Sheeba, B.J. Paul, Impact of ethylene carbonate on ion transport characteristics of PVdF–AgCF₃SO₃ polymer electrolyte system. *Mater. Res. Bull.* **44**, 1534–1539 (2009)

68. L. Fan, Z. Dang, G. Wei, C. Nan, M. Li, Effect of nanosized ZnO on the electrical properties of (PEO)₁₆LiClO₄ electrolytes. *Mater. Sci. Eng. B* **99**, 340 (2003)
69. E.M. Masoud, A.-A. El-Bellihi, W.A. Bayoumy, M.A. Mousa, Effect of nano LiAlO₂ filler on structure and electrical conduction in PEO-LiClO₄ based composite polymer electrolyte. *Mater. Res. Bull.* **48**(3), 1148–1154 (2013)
70. A.A. ElBellihi, W.A. Bayoumy, E.M. Masoud, M.A. Mousa, Preparation, characterizations and conductivity of composite polymer electrolytes based on PEO–LiClO₄ and nano ZnO filler. *Bull. Kor. Soc.* **33**(9), 2949–2954 (2012)
71. E.M. Masoud, Nano lithium aluminate filler incorporating gel lithium triflate - polymer composite: preparation, characterization and application as an electrolyte in lithium ion batteries. *Polym. Test.* **56**, 65–73 (2016)
72. E.M. Masoud, Citrated porous gel copolymer electrolyte composite for lithium ion batteries application: an investigation of ionic conduction in an optimized crystalline and porous structure. *J. Alloys Compd.* **651**, 157–163 (2015)
73. R. Prasanth, N. Shubha, H.H. Hng, M. Srinivasan, Effect of nano-clay on ionic conductivity and electrochemical properties of poly(vinylidene fluoride) based nanocomposite porous polymer membranes and their application as polymer electrolyte in lithium ion batteries. *Eur. Polym. J.* **49**, 307–318 (2013)

Publisher's Note Springer Nature remains neutral with regard to jurisdictional claims in published maps and institutional affiliations.

Springer Nature or its licensor (e.g. a society or other partner) holds exclusive rights to this article under a publishing agreement with the author(s) or other rightsholder(s); author self-archiving of the accepted manuscript version of this article is solely governed by the terms of such publishing agreement and applicable law.